Electronic Research Archive

ERA, 30(10): 3887–3901.
DOI: 10.3934/era.2022198
Received: 08 May 2022
Revised: 13 July 2022
Accepted: 14 July 2022
Published: 29 August 2022

http://www.aimspress.com/journal/ERA

Research article

Vibration analysis and multi-state feedback control of maglev vehicle-guideway coupling system

Lingling Zhang*

College of Information Science and Engineering, Hunan Women's University, Changsha 410004, Hunan, China

* **Correspondence:** Email: linglingmath@gmail.com, z002005@163.com; Tel: +073185570812.

Abstract: Due to the existence of elastic modes in the track, the suspension system of maglev train is prone to vehicle-track coupling vibration, which has become an important problem restricting the further development of maglev train technology. In view of the limitation of the existing rigid track suspension model, this paper establishes an electromagnet-controller-elastic track coupling system model. And then, the nonlinear maglev system is transformed into a linear system by Hartman-Grobman theorem. Since the elastic deformation of the track is difficult to measure, a tracking differentiator is presented to filter out the interference of the displacement signal and obtain the differential signal of the gap between the electromagnet and the track. In order to suppress the vehicle-track coupling vibration, a four-state feedback control method is proposed by introducing the gap differential feedback signal. According to the Hurwitz algebraic criterion, the stability of four-state feedback control system is compared with that of three-state feedback control system. Simulation results show that, the four-state feedback control method can provide the elastic deformation information of the track, and can suppress the coupling vibration between the vehicle and the elastic track effectively.

Keywords: maglev system; coupled vibration; elastic track; multi-state feedback control; stability

1. Introduction

Maglev train has many advantages such as high speed, low noise, small vibration and low maintenance cost, which is the development direction of modern rail transit [1]. Different from the

other wheel rail transit, maglev train relies on the electromagnet installed on the vehicle to suspend the car body above the track, so as to realize the non-contact support between the vehicle and the track. However, due to the need for active control to suspend the car body in the air, when the track is elastic, or the controller performance can't cooperate with the track well, the vehicle-track coupling vibration will occur randomly [2]. Vehicle-track coupled vibration is an important technical problem in maglev train suspension system.

In the test, the vehicle-track coupling vibration often occurs on different tracks. When TR04 of Germany and HSST04 of Japan are suspended on the steel frame bridge, the coupling vibration phenomenon of vehicle and track has been found [3]. AMT maglev train in the United States has good levitation performance in Edgewater test center, but after moving to Old Dominion University, vehicle and track coupling vibration occurs [4]. When TR08 of Germany is suspended on the steel structure track in the depot of the maintenance base, or running at a lower speed, it is prone to severe vehicle - track coupling vibration. However, when TR08 is running on the main line with a density of 7 ton/ m, the coupling vibration rarely occurs [5,6]. In engineering, although the possibility of coupling vibration can be reduced by adding up the mass and stiffness of the track, the cost of the system is significantly increased.

At present, many scholars have studied the mechanism and characteristics of vehicle-track coupling vibration. Kim et al. [7] studied the dynamic behavior of the maglev vehicle with elastic track when it was stationary or running at low speed through numerical simulation. Zhang et al. [2] studied the dynamic characteristics of magnetic levitation system with elastic guideway and velocity signal delay, and pointed out that the track elasticity is an important factor to induce the coupling vibration of the system. Wang et al. [8] proposed an on-line optimization method of control structure to suppress vibration aiming at the problem of track deformation and irregularity. Zhou et al. [9] proposed an adaptive vibration compensation method, which significantly reduces the vibration amplitude. Xu et al. [10] established the mathematical model of maglev system, and studied the dynamic behavior of maglev train on elastic track considering the state delay of position signal and speed signal of the electromagnet.

It is not difficult to find that in previous studies, some studies ignored the role of suspension controller and focused on the internal relationship between track elasticity and coupled vibration. While, some researchers only regard the track elasticity as an external disturbance, ignoring the coupling effect of the track structure and of the suspension control [11–14]. In fact, the vehicle-track coupling vibration of maglev system is closely related to the structure parameters of the track and control parameters of the controllers [11,15,16].

In order to suppress the vehicle-track coupling vibration of maglev system with flexible track, this paper propose a nonlinear stability analysis method and a multi-state feedback control method. The contributions of this paper are summarized in the following two aspects.

1) A stability analysis method for the vehicle-track coupling vibration of maglev system is presented. This method transforms the stability problem of the nonlinear maglev system with flexible track into an equivalent linear system stability problem, and the coupling vibration frequency of the system can be calculated.

2) A multi-state feedback control method with gap differential signal against the vehicle-track coupling vibration of maglev system is proposed. This method introduces the flexible track information to the control system, the vehicle-track coupling vibration of maglev train can be effectively avoided.

The remainder of this paper is organized as follows. In Section 2, the vehicle-track coupling system model considering the flexible guideway is built. In Section 3, a four-state feedback control algorithm with gap differential signal is proposed. In Section 4, the stability analysis method for the

nonlinear vehicle-track coupling system is presented. In Section 5, the effectiveness of the proposed vibration control method is verified by some simulation experiments. In this paper, by adjusting some key control parameters, the dynamic evolution behavior between the maglev train and the elastic track is comprehensively investigated, which can provide a reference for suppressing the vehicle-track coupling vibration.

2. Vehicle-track coupling suspension system modeling considering elastic track

The maglev train with electromagnetic attraction relies on the electromagnetic force provided by some electromagnets to suspend and support the carriage. Due to the distributed control of each electromagnet, the mechanical decoupling can be realized to a great extent, so the coupling effect between the electromagnets is greatly reduced. In order to simplify the research and clarify the basic characteristics of suspension system of maglev train, the model of the suspension control system with a single electromagnet is established [17–19].

Considering the elastic mode of track, the suspension control system of single electromagnet mainly includes a suspension electromagnet group, an elastic track and a suspension controller. It is the smallest unit of the suspension control system of maglev train, and can reflect the basic dynamic characteristics of the interaction between the vehicle and track [20,21].

Figure 1 is the schematic diagram of the vehicle-track coupling system of maglev train with a single electromagnet. In Figure 1, O is the left fulcrum of the track, OX is the running direction of the train; OZ is the direction of gravity acceleration, z_1 is the vertical displacement of the electromagnet, z_g is the vertical displacement of the track; m is the mass of the electromagnet, M is the mass of the carriage and passengers, l is the distance between the center of the electromagnet and the origin O in the ox direction OX. The displacement sensor is installed on the electromagnet, which measure the displacement between the track and the electromagnet as $z_1 - z_g$. F_e is the attractive force of the electromagnet.

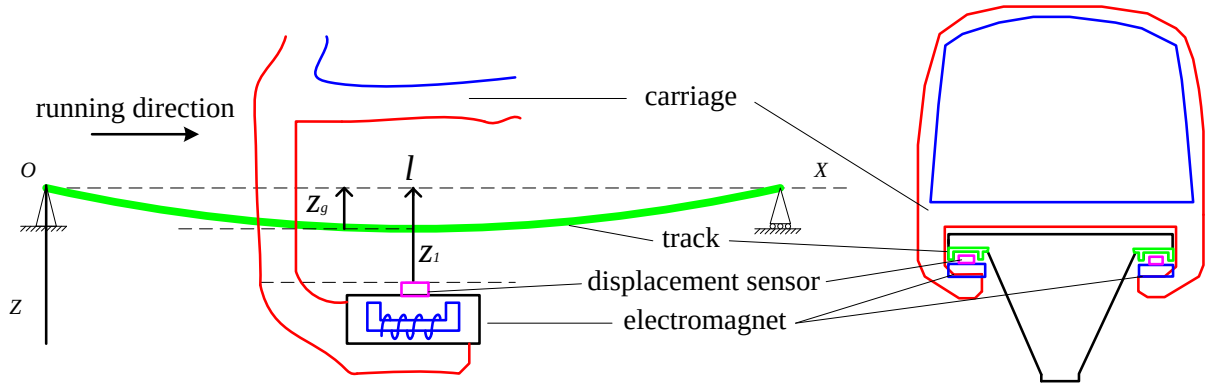

Figure 1. Suspension system model with the elastic track.

Due to the influence of track joint, track irregularity or communication error code, the displacement signal is often interrupted. Because of the discontinuity of the displacement signal, the control difficulty of suspension system of the maglev train increases greatly, and it is easy to cause the failure of the control system or the vehicle-rail coupling vibration.

2.1. Model of the elastic track

When the elastic mode of the track is considered, any point $z_g(l,t)$ of the beam satisfies the Bernoulli-Euler dynamic equation [3,11,17].

$$E_g I_g \frac{\partial^4 z_g}{\partial l^4} - T_g \frac{\partial^2 z_g}{\partial l^2} + \rho_g \frac{\partial^2 z_g}{\partial t^2} + b_g \frac{\partial z_g}{\partial t} + k_g z_g = p(l,t) \tag{1}$$

where, the parameters of the beam are given as below. E_g is the modulus of elasticity, I_g is the section inertia, T_g is the tension, ρ_g is the mass linear density, b_g is the equivalent damping coefficient, k_g is the equivalent elastic coefficient of the beam, and $p(l,t)$ is the distributed load density on the beam.

Combined with the test phenomenon, when the vehicle-track coupling vibration occurs, the vibration frequency of the track is in a certain frequency band. Because the excitation of the high-order vibration of the track needs a lot of energy, it is generally considered that the vehicle-track coupling vibration is mainly related to the first-order mode of the track.

The modal analysis method is adopted, in which only the first mode of the track is considered. Let

$$z_g(l,t) = \phi_1(l) \cdot q_1(t) \tag{2}$$

where, $\phi_1(l)$ is the first mode function, $q_1(t)$ is the generalized coordinates of the beam.

Here, l_g is the span of the beam, m_g is the mass of the track. It is known that the normalized mode function $\phi_1(l)$ is

$$\phi_1(l) = \sqrt{\frac{2}{m_g}} sin(\frac{\pi l}{l_g}). \tag{3}$$

The natural frequency of the first mode of the track is

$$\omega_1 = (\frac{\pi}{l_g})^2 \sqrt{\frac{E_g I_g}{\rho_g}}. \tag{4}$$

The first order generalized force exerted on the track is

$$\ddot{q}_1(t) + 2\eta_1\omega_1\dot{q}_1(t) + \omega_1^2 q_1(t) = Q_1, \tag{5}$$

where, η_1 is the damping ratio of the first mode.

Assuming that the length of electromagnet is far less than that of track, the electromagnetic force on the track can be regarded as a concentrated force. At this time, there is

$$Q_1 = \sqrt{\frac{2}{m_g}} sin(\frac{\pi l}{l_g}). \tag{6}$$

By combining the above Eqs (1)–(6), the coupling vibration model considering only the first mode of the track is obtained as follows

$$\ddot{z}_g + 2\eta_1\omega_1\dot{z}_g + \omega_1^2 z_g = \frac{2}{\rho_g l_g} sin^2(\frac{\pi l}{l_g}) F_e. \tag{7}$$

2.2. Model of the maglev system

The attractive force of the electromagnet is

$$F_e = \frac{\mu_0 N^2 A}{4}\left(\frac{i}{z_1 - z_g}\right)^2, \tag{8}$$

where, μ_0 is the vacuum permeability, N is the number of turns of the coil, i is the coil current, and A is the area of magnetic pole.

Let $C_1 = \frac{\mu_0 N^2 A}{4}$. The voltage of the electromagnet is

$$u = Ri + \frac{2C_1}{z_1 - z_g}i - \frac{2C_1 i}{(z_1 - z_g)^2}(\dot{z}_1 - \dot{z}_g), \tag{9}$$

where, R is the coil resistance.

Because the carriage and electromagnet rely on the air spring to realize the elastic support, when the train is stationary and suspended, only the vertical movement of the electromagnet is considered. Then

$$(m + M)g - F_e = m\ddot{z}_1. \tag{10}$$

2.3. Vehicle-track coupling system model

Let $C_2 = \frac{2C_1}{\rho_g l_g} sin^2\left(\frac{\pi x}{l_g}\right)$. By combining the above Eqs (7)–(10), the vehicle-track coupling system model considering only the first elastic mode of the track is obtained [3,11,17],

$$\begin{cases} \ddot{z}_g + 2\eta_1\omega_1\dot{z}_g + \omega_1^2 z_g = C_2\left(\frac{i}{z_1 - z_g}\right)^2 \\ (m + M)g - C_1\left(\frac{i}{z_1 - z_g}\right)^2 = m\ddot{z}_1 \\ u = Ri + \frac{2C_1}{z_1 - z_g}i - \frac{2C_1 i}{(z_1 - z_g)^2}(\dot{z}_1 - \dot{z}_g) \end{cases}. \tag{11}$$

Select $x = (x_1, x_2, x_3, x_4, x_5)^T = (z_1, \dot{z}_1, z_g, \dot{z}_g, i)^T$. The open-loop state space equation of the suspension system is obtained

$$\begin{cases} \dot{x}_1 = x_2 \\ \dot{x}_2 = \frac{m+M}{m}g - \frac{C_1}{m}\left(\frac{x_5}{x_1 - x_3}\right)^2 \\ \dot{x}_3 = x_4 \\ \dot{x}_4 = C_2\left(\frac{x_5}{x_1 - x_3}\right)^2 - 2\eta_1\omega_1 x_4 - \omega_1^2 x_3 \\ \dot{x}_5 = \frac{x_5}{x_1 - x_3}(x_2 - x_4) - \frac{R}{2C_1}(x_1 - x_3)x_5 + \frac{x_1 - x_3}{2C_1}u \end{cases}. \tag{12}$$

Obviously, the system (12) is a nonlinear system, and its stability should be analyzed according to the nonlinear system method.

3. Design of the multi-state feedback control law

The suspension control system (12) is a typical multi-variable system. In engineering, the PID control and multi-variable feedback control is usually used [5].

3.1. Design of multi-state feedback control law

In the past, the three-state combined feedback control law was often used as follows [2,15,17],

$$u = u_{ec} + k_s(x_1 - x_3 - z_0) + k_c x_5 + k_{bi} x_2, \tag{13}$$

where, u_{ec} is the initial voltage of electromagnet, k_s is the gap feedback coefficient, k_c is the current feedback coefficient, and k_{bi} is the coefficient of the electromagnet acceleration signal after integration.

The above control law does not contain the track information, so it has some limitations in suppressing vehicle-track coupling vibration [2,5]. In this paper, the gap differential signal is introduced into the control algorithm, and the feedback coefficient is k_{sd}, which is equivalent to adding the track information in the feedback control. The four-state feedback control law is

$$u = u_{ec} + k_s(x_1 - x_3 - z_0) + k_c x_5 + k_{bi} x_2 + k_{sd}(x_2 - x_4). \tag{14}$$

It can be seen from (14) that when the above control law is applied to the suspension control system, it needs to be able to obtain the five state variables x_1, x_2, x_3, x_4, x_5.

In the actual suspension system, the displacement sensor S_1, current sensor S_2 and accelerometer S_3 are installed on the electromagnet, as shown in Figure 2. Here, the displacement sensor S_1 can measure the displacement $x_1 - x_3$ between the electromagnet and the track. The current sensor S_2 can directly measure the current x_5 of the electromagnet by a low pass filter. For the accelerometer S_3, the velocity signal x_2 of the electromagnet is obtained by a high pass filter and an integrator. Although the signals x_1, x_3 can not be obtained directly by the above sensors, we can acquire the differential signals $x_2 - x_4 = \dot{x}_1 - \dot{x}_3$ indirectly by a tracking differentiator in Figure 2.

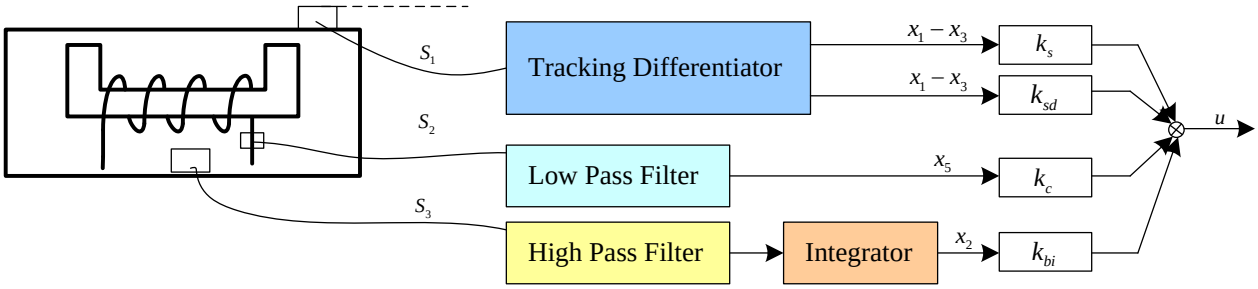

Figure 2. Block diagram of the four-state feedback control law.

3.2. Design of the tracking differentiator

In engineering, it is very important to extract the differential signal from the original signal. For the magnetic suspension system, whether using PID control or multi-state feedback control, we both

need to use the appropriate differential signal.

In the past magnetic levitation system, the differential signal extracted from the relative displacement of electromagnet and track can not be used directly. The main reason is the obvious increase of noise.

Assume that the original signal is v. The traditional differential signal is obtained by the following differential link

$$\dot{v} = w(s)v = \frac{s}{Ts+1}v, \tag{15}$$

where, T is a relatively small time constant.

In order to reduce the noise amplification effect, in Figure 2, an improved tracking differentiator is used to extract the differential signal [15,16].

$$\dot{v} = w(s)v = \frac{s}{\tau_1\tau_2 s^2+(\tau_1+\tau_2)s+1}v \tag{16}$$

where, τ_1, τ_2 are relatively small time constant, and $0 < \tau_1 < \tau_2$.

Here, $T = 0.001$, $\tau_1 = 0.01, \tau_2 = 0.02, N = 2000, v = sin\, t + 0.0002rand(1, N)$. Using (15) and (16), the corresponding differential signals are obtained respectively, as shown in Figures 3.

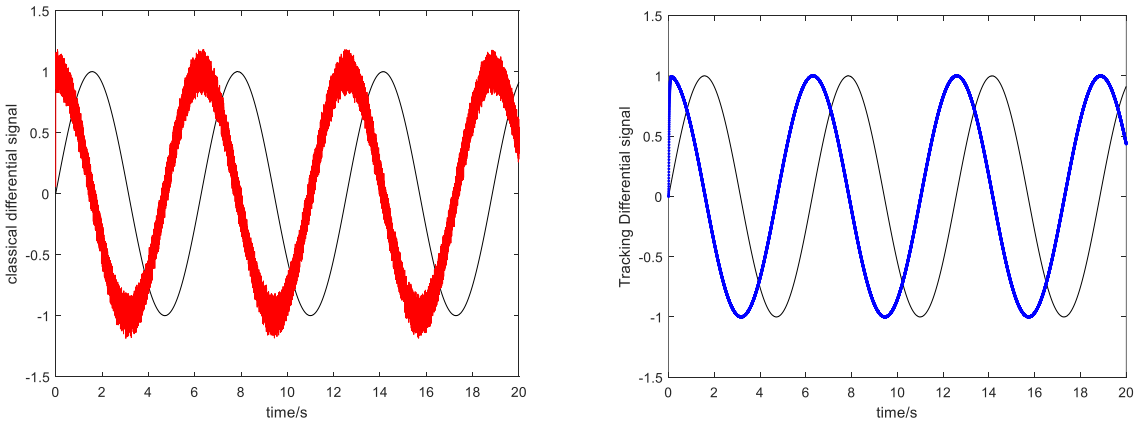

(a) (b)

Figure 3. Comparison of output signals of traditional differentiator and tracking differentiator.

4. Stability analysis

4.1. Stability analysis of closed loop system

By substituting the state feedback (14) into the open-loop state system (12), the following closed-loop state space equation of the system is obtained [11,17]:

$$\begin{cases} \dot{x}_1 = x_2 \\ \dot{x}_2 = \frac{m+M}{m} g - \frac{C_1}{m} (\frac{x_5}{x_1 - x_3})^2 \\ \dot{x}_3 = x_4 \\ \dot{x}_4 = C_2 (\frac{x_5}{x_1 - x_3})^2 - 2\eta_1 \omega_1 x_4 - \omega_1^2 x_3 \\ \dot{x}_5 = \frac{x_5}{x_1 - x_3} (x_2 - x_4) - \frac{R}{2C_1} (x_1 - x_3) x_5 + \frac{x_1 - x_3}{2C_1} (u_{ec} + k_s (x_1 - x_3 - z_0) \\ \qquad\qquad + k_c x_5 + k_{bi} x_2 + k_{sd} (x_2 - x_4)) \end{cases} . \tag{17}$$

For the system (17), let $\dot{x} = (x_1, x_2, x_3, x_4, x_5)^T = 0$, and define $C_3 = \sqrt{\frac{(m+M)g}{C_1}}$, the singular point of the system can be obtained as follows

$$x_0 = (\frac{C_2 C_3^2}{\omega_1^2} + z_0, 0, \frac{C_2 C_3^2}{\omega_1^2}, 0, z_0 C_3)^T. \tag{18}$$

It is not difficult to find that the equilibrium point of the four-state feedback system with gap differential information is the same as that of the three-state feedback system without gap differential information. Therefore, the four-state feedback with gap differential information does not change the static operating point of the system.

At the equilibrium point, we have $x_1 - x_3 = z_0$. Further, the initial static voltage u_{ec0} of the electromagnet is obtained as

$$u_{ec0} = (R - k_c) z_0 C_3. \tag{19}$$

In fact, its size determines the size of the suspension gap in the stable state.

At the equilibrium point x_0, the system (17) is linearized and the Jacobian matrix of the system is

$$J = \begin{bmatrix} 0 & 1 & 0 & 0 & 0 \\ \frac{2C_1 C_3^2}{m z_0} & 0 & -\frac{2C_1 C_3^2}{m z_0} & 0 & -\frac{2C_1 C_3}{m z_0} \\ 0 & 0 & 0 & 1 & 0 \\ -\frac{2C_2 C_3^2}{z_0} & 0 & \frac{2C_2 C_3^2}{z_0} - \omega_1^2 & -2\eta_1 \omega_1 & \frac{2C_2 C_3}{z_0} \\ \frac{z_0 k_s}{2C_1} & C_3 + \frac{z_0 (k_{bi} + k_{sd})}{2C_1} & -\frac{z_0 k_s}{2C_1} & -C_3 - \frac{z_0 k_{sd}}{2C_1} & -\frac{z_0 (R - k_c)}{2C_1} \end{bmatrix}. \tag{20}$$

In this way, the nonlinear system (17) at the equilibrium point can be expressed as

$$\dot{x} = J(x_0)(x - x_0) + O(x - x_0), x \in R^n, \tag{21}$$

where, $O(x - x_0)$ is a higher order infinitesimal.

Lemma 1. There is a nonlinear system (17) and its corresponding linear system (21) at the equilibrium point. If x_0 is an isolated singular point of system (17) and all eigenvalues of $J(x_0)$ have non-zero real parts, it is called x_0 is a hyperbolic singular point of system (17). While, if some eigenvalues of $J(x_0)$ have zero real parts, it is called x_0 is a non-hyperbolic singular point of system (17).

Theorem 1 [11,17]. (Hartman Grobman Theory) if x_0 is a hyperbolic singular point of system (17) and satisfies the condition.

$$\lim_{x\to x_0}\frac{O(x-x_0)}{|x-x_0|}=0, x\in R^n \tag{22}$$

Then the system (17) has the same topological structure as the corresponding linear system (21) at the isolated singular point x_0.

The above theorem is also called the first approximation theorem. According to the theorem, for the nonlinear vehicle-track coupling control system (17) of maglev train, if its equilibrium point is hyperbolic singularity, we only need to analyze its linear system at the equilibrium point, and then we can get the stability of nonlinear system (17) near the equilibrium point.

The characteristic polynomial of Eq (20) is

$$J(\lambda)=\lambda^5+a_1\lambda^4+a_2\lambda^3+a_3\lambda^2+a_4\lambda+a_5 \tag{23}$$

where, $a_1=2\eta_1\omega_1-\frac{z_0(k_c-R)}{2C_1}$, $a_2=\omega_1^2+\frac{C_3k_{bi}}{m}-\frac{\eta_1\omega_1z_0(k_c-R)}{C_1}+\frac{C_3k_{sd}}{m}+\frac{C_2C_3k_{sd}}{C_1}$, $a_3=\frac{C_3k_s}{m}+\frac{C_2C_3^2(k_c-R)}{C_1}+\frac{C_2C_3k_s}{C_1}+\frac{2C_3\eta_1\omega_1k_{bi}}{m}-\frac{\omega_1^2z_0(k_c-R)}{2C_1}+\frac{C_3^2k_s}{m}+\frac{2C_3\eta_1\omega_1k_{sd}}{m}$, $a_4=\frac{2C_3^2\eta_1\omega_1(k_c-R)}{m}+\frac{2C_3\eta_1\omega_1k_s}{m}+\frac{C_3\omega_1^2k_{bi}}{m}+\frac{C_3\omega_1^2k_{sd}}{m}$, $a_5=\frac{C_3^2\omega_1^2(k_c-R)}{m}+\frac{C_3\omega_1^2k_s}{m}$.

Because of the complexity of the characteristic polynomial, it is difficult to obtain the analytical solution of the system directly. The stability of the system can be analyzed by Hurwitz criterion.

The Hurwitz determinant is constructed as follows

$$\Delta_5=\begin{vmatrix}a_1 & 1 & 0 & 0 & 0\\ a_3 & a_2 & a_1 & 1 & 0\\ a_5 & a_4 & a_3 & a_2 & a_1\\ 0 & 0 & a_5 & a_4 & a_3\\ 0 & 0 & 0 & 0 & a_5\end{vmatrix}. \tag{24}$$

Lemma 2. (Hurwitz criterion) the linear system (21) corresponding to matrix (20) is asymptotically stable, that is, all eigenvalues of characteristic polynomial (23) have negative real parts, if and only if $a_1>0,\ a_2>0,\ a_3>0,\ a_4>0,\ a_5>0$, and $\Delta_2=a_1a_2-a_3>0$,

$$\Delta_4=\begin{vmatrix}a_1 & 1 & 0 & 0\\ a_3 & a_2 & a_1 & 1\\ a_5 & a_4 & a_3 & a_2\\ 0 & 0 & a_5 & a_4\end{vmatrix}>0. \tag{25}$$

Lemma 2 shows that the linear system (23) corresponding to the nonlinear system (17) at the equilibrium point is asymptotically stable, which also means that the nonlinear system (17) is asymptotically stable near the equilibrium point.

4.2. Analysis of vehicle-track coupling vibration

It is generally believed that when the vehicle-track coupling vibration occurs, the system is in a critical stable state, and the corresponding linear system may have a Hopf bifurcation point.

Theorem 2 [11,17]. The linear system (21) corresponding to the matrix (20) is in a critical stable state, that is, the characteristic polynomial (20) has a pair of pure imaginary roots $\pm j\omega$, and the other

three characteristic roots all have negative real parts, if and only if $a_1 > 0,\ a_2 > 0,\ a_3 > 0,\ a_4 > 0,$ $a_5 > 0$, and $\Delta_2 = a_1 a_2 - a_3 > 0,\ \Delta_4 = \begin{vmatrix} a_1 & 1 & 0 & 0 \\ a_3 & a_2 & a_1 & 1 \\ a_5 & a_4 & a_3 & a_2 \\ 0 & 0 & a_5 & a_4 \end{vmatrix} = 0$. Here, $\omega = \sqrt{\frac{a_2 a_5}{a_3}}$.

From Theorem 2, the possible Hopf bifurcation point of the system can be obtained.

5. System simulation

The parameters of the suspension system of a maglev train are as follows.

$m = 500kg,\ M = 1000kg,\ R = 4\Omega,\ \eta_1 = 0.005,\ \omega_1 = 50\pi,\ C_1 = 0.0026,\ C_2 = 4e-8, l_g = 25m, z_0 = 0.010m, l_e = 3m.$ The initial value is $x = (0.020,0,0.0002,0,0)$.

1) The system is in critical stable state without gap differential signal.

At this time, select the control parameter as $k_c = -40,\ k_{bi} = 800,\ k_s = 172{,}321,\ k_{sd} = 0,$ and get the response curve of the system, as shown in Figure 4. Figure 4(a) is the displacement curve of electromagnet, Figure 4(b) is the displacement curve of track, Figure 4(c) is the relative displacement curve of electromagnet and track, and Figure 4(d) is the phase trajectory diagram of relative displacement of electromagnet and track.

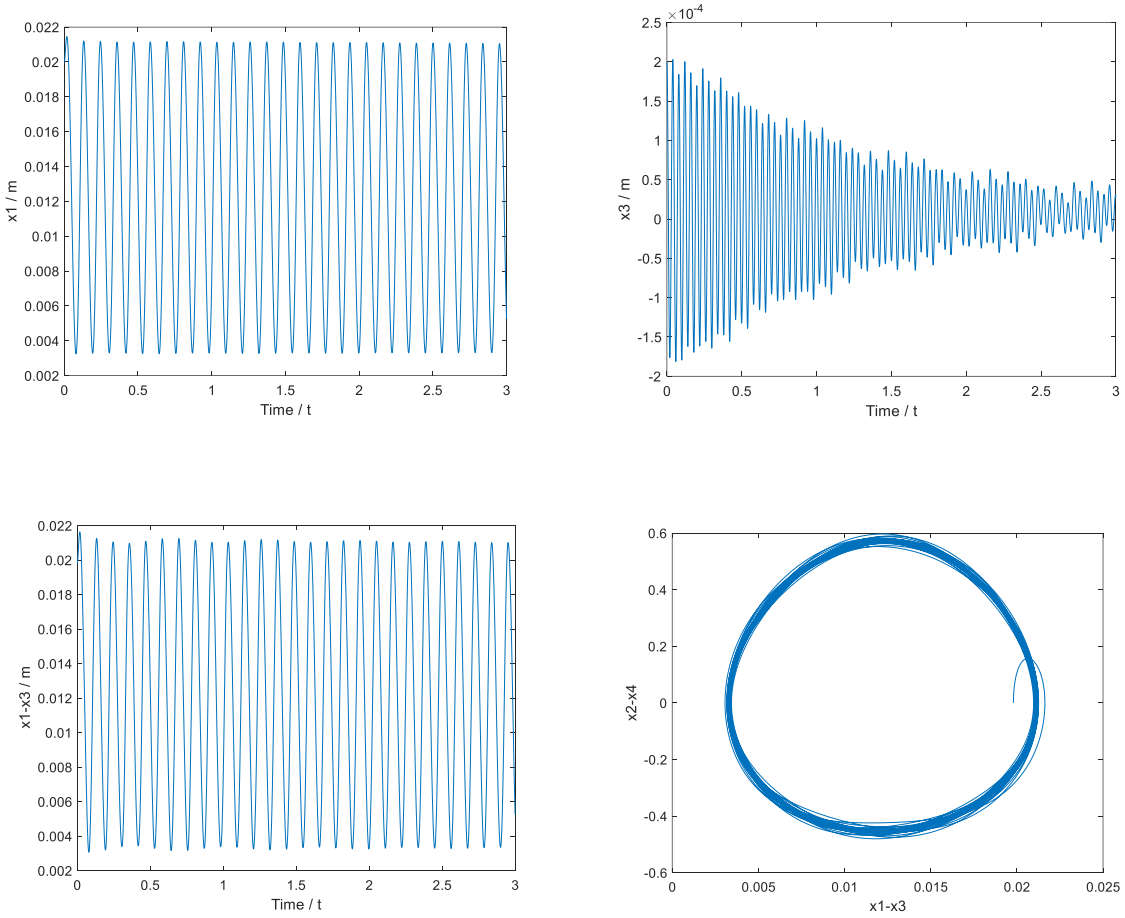

Figure 4. Response curve of the system in a critical stable state with $\boldsymbol{k_s = 172,321,\ k_{sd} = 0}$.

It can be seen from Figure 4 that when $k_s = 172{,}321,\ k_{sd} = 0$, the suspension system was in a critical stable state at that time. It can be seen from Figure 4(c) that the relative displacement between the electromagnet and the track is in a state of constant amplitude oscillation. If the control is not adopted effectively in time, the coupled vibration will occur continuously. From Theorem 2, we can get $a_1 > 0,\ a_2 > 0,\ a_3 > 0,\ a_4 > 0,\ a_5 > 0$, and $\Delta_2 = a_1 a_2 - a_3 > 0$. At that time, when $\Delta_4 = 0$, we get $\omega_0 = 50.3\pi$. The value is very close to the first-order frequency of the track and the simulation result in Figure 4(b). It is not difficult to find that the coupling vibration frequency is $\omega_0 = 50.1\pi$.

2) The system is in a stable state without gap differential signal.

At this time, the control parameter is selected as $k_c = -40,\ k_{bi} = 800,\ k_s = 179{,}035,\ k_{sd} = 0$, and the response curve of the system is obtained, as shown in Figure 5. Figure 5(a) is the displacement curve of electromagnet, Figure 5(b) is the displacement curve of track, Figure 5(c) is the relative displacement curve of electromagnet and track, and Figure 5(d) is the phase trajectory diagram of relative displacement of electromagnet and track.

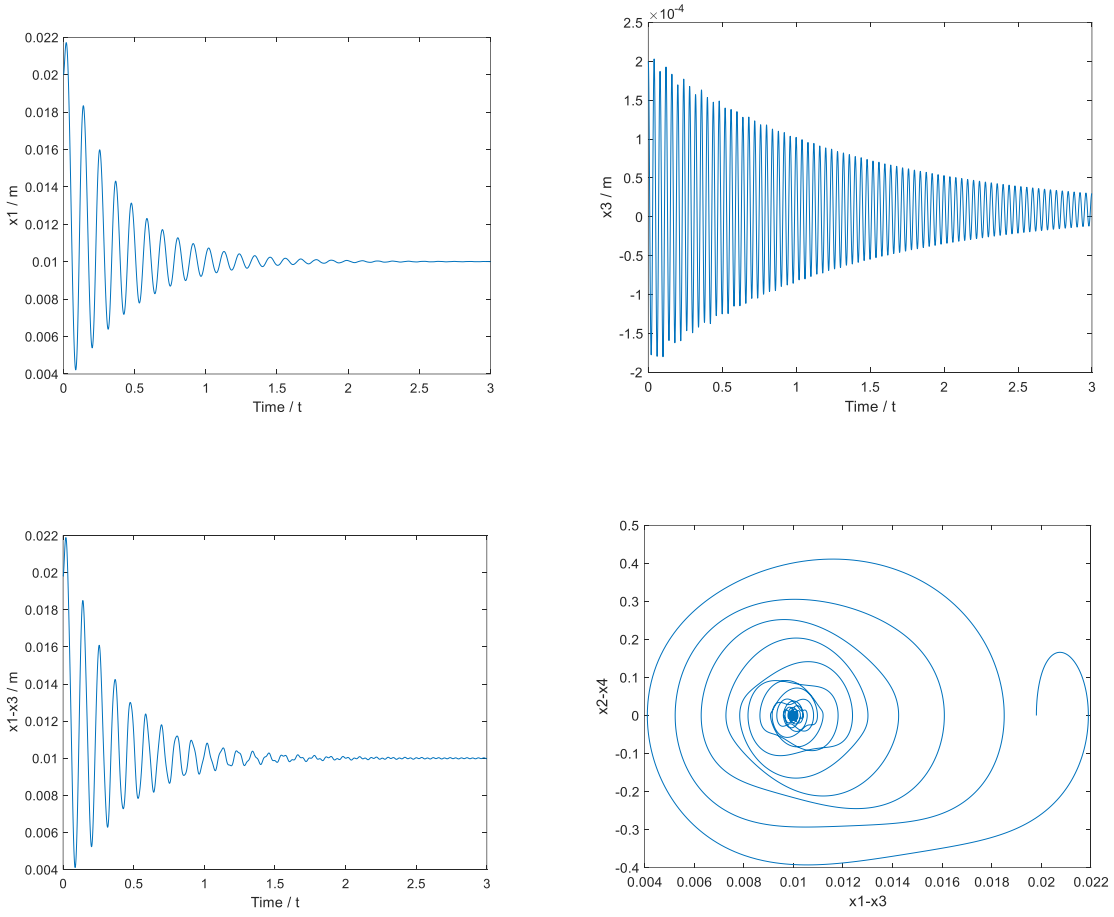

Figure 5. Response curve of the system in a stable state with $\boldsymbol{k_s = 179{,}035,\ k_{sd} = 0}$.

It can be seen from Figure 5 that, when $k_s = 179{,}035,\ k_{sd} = 0$, the suspension system can reach a stable working state at that time. From Figure 5(c) that after 1.4 seconds, the relative displacement fluctuation range between the electromagnet and the track is less than 2 mm, realizing stable suspension.

3) The system is in a stable state with gap differential signal.

At this time, the control parameter is selected as $k_c = -40$, $k_{bi} = 800$, $k_s = 172{,}321$, $k_{sd} = 200$, and the response curve of the system is obtained, as shown in Figure 6. Figure 6(a) is the displacement curve of electromagnet, Figure 6(b) is the displacement curve of track, Figure 6(c) is the relative displacement curve of electromagnet and track, and Figure 6(d) is the phase trajectory diagram of relative displacement of electromagnet and track.

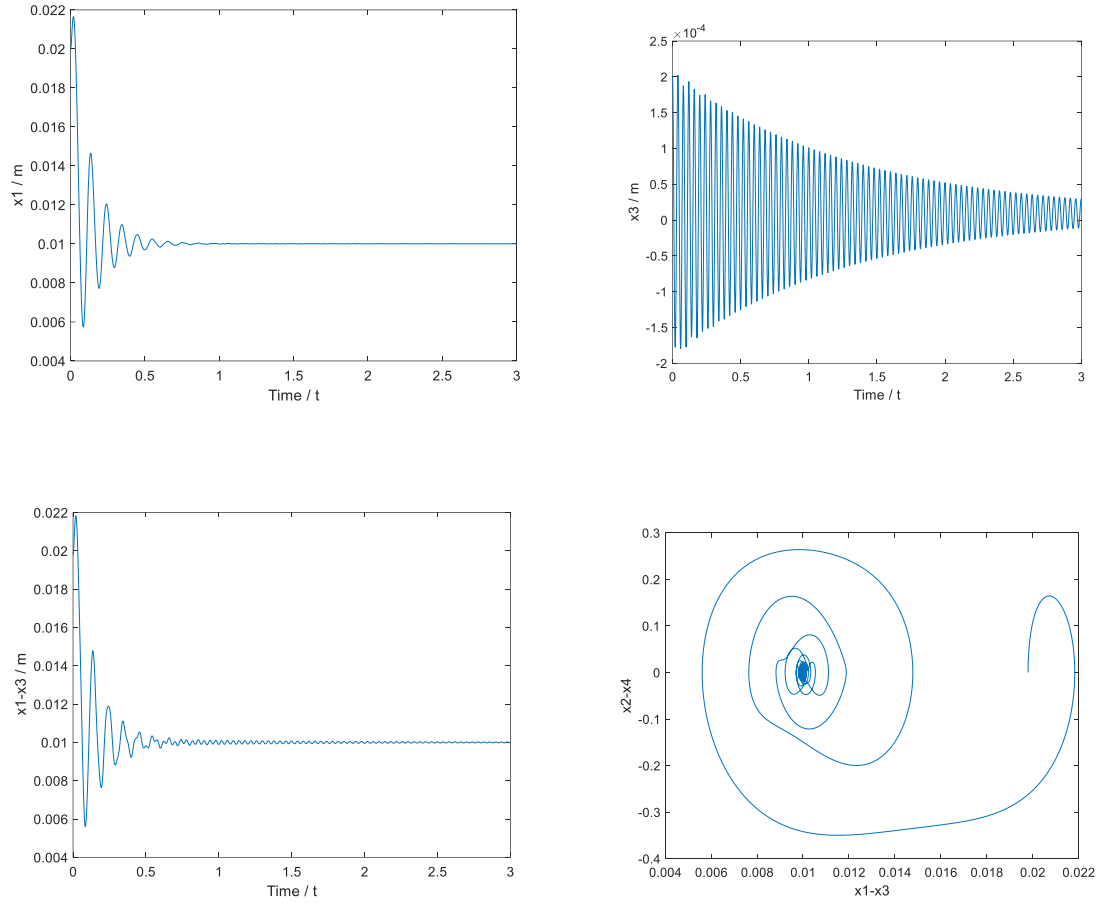

Figure 6. Response curve of the system in a stable state with $\boldsymbol{k_s = 172,321}$, $\boldsymbol{k_{sd} = 200}$.

It can be seen from Figure 6 that the suspension system was still in a stable working state at that time. As can be seen from Figure 6(c), after 0.5 seconds, the relative displacement fluctuation range between the electromagnet and the track is less than 1 mm, realizing stable suspension.

Notation: For the magnetic levitation system, the performance differences of different control methods are mainly reflected in the convergence speed and steady-state fluctuation range of the vertical displacement x_1 of the electromagnet. In Figure 5(a), with the three-state combined feedback control method, the convergence speed of x_1 is 1.6 s and steady-state fluctuation range of x_1 is 2 mm. While, in Figure 6(a), with the four-state improved feedback control method, the convergence speed of x_1 is 0.7 s and steady-state fluctuation range of x_1 is 1 mm.

Through the above analysis, it can be seen that the system may be in a critical stable state when there is no gap differential signal feedback, and the vehicle and track will continue to vibrate. After introducing the gap differential signal to the feedback control law, the regulation time of the system is

shortened and the stability is improved.

6. Conclusions and discussion

Aiming at the problem of vehicle-track coupling vibration in maglev train suspension system, a four-state feedback control algorithm is proposed in this paper. By investigating the dynamic evolution behavior of the interaction between structure parameters and control parameters of the suspension system, the vehicle-track coupling vibration of maglev train has been effectively avoided.

In order to fully describe the real dynamic characteristics of the system, this paper fully considers the elastic modal factors of the track, and establishes a coupling system model with elastic track. Furthermore, by using the first approximation theorem, the stability problem of the nonlinear maglev system is transformed into an equivalent linear system stability problem. Then, the gap differential signal is introduced to the feedback system, and a four-state feedback control strategy is adopted to the magnetic suspension system. According to the Hurwitz algebraic criterion, the coupling vibration frequency of the system can be calculated, and the coupling vibration of the system can be judged. The above research provides a useful reference for effectively suppressing the coupling vibration between vehicle and elastic track.

In this paper, only the first order vibration mode is considered. In fact, the results will be closer to the actual situation when the higher order vibration mode is considered. Further, the above four-state feedback control algorithm method will be applied to the practical maglev system to verify its feasibility.

Acknowledgments

The authors would like to thank the referees for their comments and suggestions which helped to improve the manuscript. This work was supported by the Scientific Research Key Project of Hunan Provincial Education Department (20A267).

Conflict of interest

The authors declare no conflict of interest. The founding sponsors had no role in the design of the study; in the collection, analyses, or interpretation of data; in the writing of the manuscript, and in the decision to publish the results.

References

1. H. W. Lee, K. C. Kim, J. Lee, Review of maglev train technologies, *IEEE Trans. Magn.,* **42** (2006), 1917–1925. https://doi.org/10.1109/TMAG.2006.875842
2. Z. Z. Zhang, L. L. Zhang, Hopf bifurcation of time-delayed feedback control for maglev system with flexible guideway, *Appl. Math. Comput.,* **219** (2013), 6106–6112. https://doi.org/10.1016/j.amc.2012.12.045
3. J. H. Li, J. Li, P. C. Yu, Saturation influence of control voltage on maglev stationary self-excited vibration, *J. Cent. South Univ.,* **23** (2016), 1954–1960. https://doi.org/10.1007/s11771-016-3252-4

4. Y. G. Sun, J. Q. Xu, H. Y. Qiang, W. J. Wang, G. B. Lin, Hopf bifurcation analysis of maglev vehicle-guideway interaction vibration system and stability control based on fuzzy adaptive theory, *Comput. Ind.*, **108** (2019), 197–209. https://doi.org/10.1016/j.compind.2019.03.001
5. L. H. She, Z. Z. Zhang, D. S. Zou, W. S. Chang, Multi-state feedback control strategy for maglev elastic vehicle-guideway-coupled system, *Adv. Sci. Lett.*, **5** (2012), 587–592. https://doi.org/10.1166/asl.2012.1772
6. L. L. Zhang, L. H. Huang, Z. Z. Zhang, Hopf bifurcation of the Maglev time-delay feedback system via pseudo-oscillator analysis, *Math. Comput. Modell.*, **52** (2010), 667–673. https://doi.org/10.1016/j.mcm.2010.04.014
7. K. J. Kim, J. B. Han, H. S. Han, S. J. Yang, Coupled vibration analysis of maglev vehicle-guideway while standing still or moving at low speeds, *Veh. Syst. Dyn.*, **53** (2015), 587–601. https://doi.org/10.1080/00423114.2015.1013039
8. Z. Q. Wang, Z. Q. Long, X. L. Li, Track irregularity disturbance rejection for maglev train based on online optimization of PnP control architecture, *IEEE Access*, **7** (2019), 12610–12619. https://doi.org/10.1109/ACCESS.2019.2891964
9. D. F. Zhou, P. C. Yu, L. C. Wang, J. Li, An adaptive vibration control method to suppress the vibration of the maglev train caused by track irregularities, *J. Sound Vib.*, **408** (2017), 331–350. https://doi.org/10.1016/j.jsv.2017.07.037
10. J. Q. Xu, C. Chen, D. G. Gao, S. H. Luo, Q. Q. Qian, Nonlinear dynamic analysis on maglev train system with flexible guideway and double time-delay feedback control, *J. Vibroeng.*, **19** (2017), 6346–6362. https://doi.org/10.21595/jve.2017.18970
11. X. H. Shi, Z. Q. Long, Nonlinear vibration analysis of the maglev guideway-vehicle coupling control system, *J. China Railw. Soc.*, **31** (2009), 38–42.
12. Z. Q. Wang, Z. Q. Long, Y. D. Xie, J. F. Ding, J. Luo, X. L. Li, A discrete nonlinear tracking-differentiator and its application in vibration suppression of maglev system, *Math. Probl. Eng.*, **2020** (2020). https://doi.org/10.1155/2020/1849816
13. Z. Z. Zhang, L. L. Zhang, L. H. She, Z. Q. Long, Fuzzy integrality design for maglev networked control system with sensor data dropouts, *Appl. Mech. Mater.*, **44–47** (2010), 1437–1441. https://doi.org/10.4028/www.scientific.net/AMM.44-47.1437
14. Y. Zhang, L. L. Zhang, Intelligent fault detection of reciprocating compressor using a novel discrete state space, *Mech. Syst. Sig. Process.*, **169** (2022), 108583. https://doi.org/10.1016/j.ymssp.2021.108583
15. Z. Z. Zhang, Applied adaptive controller design for vibration suppression in electromagnetic systems, *Appl. Comput. Electromagn. Soc. J.*, **34** (2019), 567–576.
16. Z. Z. Zhang, X. L. Li, Real-time adaptive control of a magnetic levitation system with a large range of load disturbance, *Sensors*, **18** (2018), 1512–1526. https://doi.org/10.3390/s18051512
17. L. L. Zhang, Z. Z. Zhang, L. H. Huang, Double Hopf bifurcation of time-delayed feedback control for maglev system, *Nonlinear Dyn.*, **69** (2012), 961–967. https://doi.org/10.1007/s11071-011-0317-7
18. S. M. Wang, Y. Q. Ni, Y. G. Sun, Y. Lu, Y. F. Duan, Modelling dynamic interaction of maglev train-controller-rail-bridge system by vector mechanics, *J. Sound Vib.*, **533** (2022), 117023. https://doi.org/10.1016/j.jsv.2022.117023
19. Y. G. Sun, S. M. Wang, Y. Lu, J. Q. Xu, S. Xie, Control of time delay in magnetic levitation systems, *IEEE Magn. Lett.*, **13** (2022), 1–5. https://doi.org/10.1109/LMAG.2021.3123909

20. Y. G. Sun, S. M. Wang, Y. Lu, J. Q. Xu, Gaussian process dynamic modeling and backstepping sliding mode control for magnetic levitation system of maglev train, *J. Theor. Appl. Mech.*, **60** (2022), 49–62. https://doi.org/10.15632/jtam-pl/143676
21. Z. Z. Zhang, Z. L. Wei, B. W. Nie, Y. Li, Discontinuous maneuver trajectory prediction based on HOA-GRU method for the UAVs, *Electron. Res. Arch.*, **30** (2022), 3111–3129. https://doi.org/10.3934/era.2022158

AIMS Press

©2022 the Author(s), licensee AIMS Press. This is an open access article distributed under the terms of the Creative Commons Attribution License (http://creativecommons.org/licenses/by/4.0)